applied sciences

MDPI

Article

Optimization Methodologies for Analyzing the Impact of Operational Parameters on a Light-Duty Methane/Diesel Reactivity-Controlled Compression Ignition (RCCI) Engine

Anwer Hamed Salih Alattwani *, Mehmet Zafer Gul and Mustafa Yilmaz

Department of Mechanical Engineering, Marmara University, Istanbul 34840, Turkey; zgul@marmara.edu.tr (M.Z.G.); mustafa.yilmaz@marmara.edu.tr (M.Y.)
* Correspondence: anweralattwani@marun.edu.tr

Abstract: This study aims to evaluate and optimize the influences of operational factors, including the engine's rotational speed, methane mass, diesel mass, and the duration of injected diesel fuel on the methane/diesel reactivity-controlled compression ignition (RCCI) light-duty engine's performance and emissions by executing the Nondominated Sorting Genetic Algorithm-II (NSGAII). The optimizations aimed to minimize peak firing pressure simultaneously, decrease indicated specific fuel consumption, and reduce tailpipe emissions. It is found that the excess air ratios of (2.22 to 2.37) are the range of feasible results of the RCCI engine, and the power should be less than 0.89 from the maximum design load of the diesel engine when it works without it after treatment. The methane/diesel RCCI engine achieves an indicative thermal efficiency of 51%. The Pareto results from the NSGA algorithm occur on multiple fronts, and there is a tradeoff between power and nitrogen oxide (NOx) in addition to unburned hydrocarbons (UHCs) and carbon monoxide (CO) with NOx emissions. Moreover, EURO IV emissions regulations can occur when using a start of injection (SOI) of −35 CA, a diesel mass of 1.82 mg, a methane mass of 9.74 mg, a diesel injection duration of 2.63 CA, and a rotational speed of 2540 rpm. This accomplished a reduction in indicative specific fuel consumption by 27.8%, higher indicative efficiency by 21.9%, and emissions reductions compared to a conventional diesel engine.

Keywords: RCCI engine; optimization; NSGAII; n-heptane; methane; emissions; excess air ratio

check for updates

Academic Editor: Adrian Irimescu

Received: 5 March 2025
Revised: 24 March 2025
Accepted: 25 March 2025
Published: 1 April 2025

Citation: Alattwani, A.H.S.; Zafer, M.; Yilmaz, M. Optimization Methodologies for Analyzing the Impact of Operational Parameters on a Light-Duty Methane/Diesel Reactivity-Controlled Compression Ignition (RCCI) Engine. *Appl. Sci.* **2025**, *15*, 3849. https://doi.org/10.3390/app15073849

Copyright: © 2025 by the authors. Licensee MDPI, Basel, Switzerland. This article is an open access article distributed under the terms and conditions of the Creative Commons Attribution (CC BY) license (https://creativecommons.org/licenses/by/4.0/).

1. Introduction

With progressively increasing strict emission rules due to collapsing atmosphere conditions, decreasing internal combustion engine tailpipe emissions have become a hotspot point for researchers. Since diesel combustion is naturally heterogeneous, diesel engines are considered the primary source of contamination. They release significant pollutants, such as carbon monoxide (CO), nitrogen oxide (NOx), unburned hydrocarbons (UHCs), and particulate matter (soot) [1–5]. Low-temperature combustion (LTC) is a modern combustion strategy that has emerged recently. It encompasses various techniques, including partially premixed compression ignition (PPCI), homogeneous charge compression ignition (HCCI), and reactivity-controlled compression ignition (RCCI). Employing LTC techniques in diesel engines can result in lower NOx and soot emissions while preserving higher efficiency when compared to traditional diesel engines. The HCCI technique relies on the auto-ignition of a fully premixed air–fuel mixture [6–8]. The PPCI method combines HCCI and traditional diesel engine combustion modes. Diesel fuel is injected near the top dead

center, avoiding the cylinder wall. In PCCI mode, cooled exhaust gas recirculation (EGR) and a low compression ratio are employed to prolong the ignition delay (ID) and lower the combustion temperature, which helps reduce NOx and soot emissions [9–11]. The RCCI combustion strategy is an advanced method derived from the PCCI approach. In this technique, a high-reactivity fuel, such as diesel, is directly injected into the cylinder in one or more stages, and the low-reactivity fuel, such as methane (CH_4), hydrogen (H_2), or gasoline, is injected through the intake port. This method leverages the varying reactivities of the fuels to control the combustion timing and duration, offering more precise control over the combustion process than other methods. This technique employs the effect of varying reactivities of fuels to regulate the combustion phase and duration, and it gives more control over combustion than the other approaches [12–17]. Methane is considered a promising low-reactivity fuel due to its distinct features, including a poor hydrogen-to-carbon ratio, less ringing intensity and high resistance to knock, higher heating value, less carbon footprint, less adiabatic flame temperature, and fewer tailpipe emissions, making it a clean fuel favorable for internal combustion engine compared with other fossil fuels. Moreover, it is available, has a lower price, has no challenges related to infrastructure, and has no evaporation loss [18]. Table 1 compares methane and n-Heptane fuels' physical and chemical properties [19]. Jia, Z., and Denbratt concluded in their study that when using a CR of 17, CA50 advanced before TDC. A TDC can be delayed by raising the amount of EGR, which results in rising UHC emissions. To maintain an acceptable amount of UHC emissions, a lower compression ratio of 14 can be used to retard the CA50 [20]. Doosje et al. revealed in their article that NOx and soot emissions were attained consistently with Euro-VI when the RCCI engine ran at 1200–1800 rpm and 2 to 9 bar BMEP in the absence of EGR. The exhaust temperatures were maintained at a low level for the suitable reduction in total UHC emissions by employing catalytic after treatment. Furthermore, the thermal efficiency of the RCCI engine was either similar to or exceeded that of a conventional diesel engine [21]. Walker et al. reported that methane/diesel fueling results in a significant load enhancement weighed against gasoline/diesel fueling for RCCI engines. The highest IMEP of 17.3 bar was accomplished when the CA50 occurred at 4 degrees after the top dead center. The findings demonstrate that the load limit can be increased through the utilization of a dual-fuel methane/diesel RCCI engine [22]. Pedrozo et al. stated that natural gas's lowest methane number (MN) reduced overall UHC emissions and methane slip. However, this betterment was combined with increased NOx emissions. Furthermore, the combination of RCCI combustion and the late-intake valve closing (LIVC) strategy can lead to reductions of up to 80% in methane slip and nitrogen oxide (NOx) emissions while simultaneously achieving relatively higher net indicated efficiency compared to the conventional dual-fuel operation [23]. In their study, Paykani et al. suggested increasing the proportion of natural gas in the fuel mixture, advancing the start timings of both the first and second injections beyond a certain threshold, and enhancing the fuel fraction during the first injection phase to reduce soot and NOx emissions. However, this approach had a detrimental effect on UHC and CO emissions [24]. Wu et al. disclosed that using natural gas with high methane numbers will reduce the combustion time, and the ignition delay will be extended in NG/diesel RCCI engine. Additionally, the impact of the methane number on UHC and CO emissions in RCCI mode remains uncertain. Furthermore, combustion phasing has a greater influence on NOx missions than the composition of natural gas in RCCI operation [25]. Nieman et al. performed an optimization study on a heavy-duty single-cylinder diesel engine, comparing the performance of methane/diesel and gasoline/diesel RCCI configurations. The multi-dimensional CFD code, KIVA3V, is coupled with the Nondominated Sorting Genetic Algorithm (NSGA-II) using the CHEMKIN chemistry tool to carry out the optimization study for an immense range of operational parameters. Engine operational parameters,

including the double injection timing of diesel, diesel pressure, the methane mass, and the amount of the EGR fraction while the objective was to minimize NOx, UHC, CO, and soot, NOx, and CO emissions, together with ringing intensity and ISFC, are used to control by the NSGA-II. The study concluded that methane is a superior choice as a low-reactivity fuel compared to gasoline for RCCI mode, primarily due to the greater reactivity difference, which aids in controlling the peak pressure rise. However, despite this advantage, the efficiency of the gasoline/diesel configuration is 2% higher than the methane/diesel configuration, attributable to the higher flame temperature of methane, which results in greater energy losses; in contrast, the methane/diesel RCCI mode produced lower NOx emissions. Furthermore, methane in the RCCI engine promotes smooth, clean, and efficient combustion. A minimal amount of soot and NOx emissions was achieved up to a load of 13.5 bar IMEP without the need for EGR. However, at higher loads, the study found that both combustion characteristics and tailpipe emissions were highly sensitive to the diesel mass in both injection phases [26]. Ansari A. et al. conducted an optimization study on a light-duty, inline four-cylinder dual-fuel RCCI engine operating on diesel and natural gas, which works on a load range from 3 to 12 bar IMEP. A design experiment (DOE) (2^3 factorial design) was executed to discover the effect of input parameters to control the desired outputs. The objectives and constraints are limited to meeting light-duty tailpipe emissions standard Tier 3 Bin 20. This optimization is employed with and without the execution of the after-treatment system while decreasing operational costs by minimizing the usage of brake-specific fuel and brake-specific urea. The study concluded that the urea fuel cost for operating the RCCI engine at higher loads (IMEP > 6 bar) was found to be 30–35% lower than that of a conventional diesel engine. Additionally, the optimal exhaust gas temperature range for CDC-RCCI operation was identified as 400–425 °C, as this allows the diesel oxidation catalyst (DOC) and selective catalytic reduction (SCR) system to operate with high efficiency, ensuring compliance with EPA emission regulations. At intermediate loads of 7–9 bar IMEP, enhanced combustion efficiency was attained along with reduced particulate matter (PM) and NOx emissions; however, this was accompanied by an increase in CO and UHC emissions [27]. Ebrahimi, M. et al. used an artifice neural network (ANN) to figure out the effect of the operational parameters, examining the effects of both intake temperature and pressure at the intake valve closing (IVC), as well as the start of injection (SOI) of diesel fuel, on the performance of a single-cylinder, heavy-duty (methane/diesel) dual-fuel RCCI engine operating at a 9.4 bar IMEP load. The outcome suggested that the fractional factorial method can generate a proper dataset for training ANN. Moreover, using artificial neural networks as an effective tool facilitates the prediction of the occurrence of misfires, excessive combustion noise, and the favored range of engine load [28]. Kakaee et al. conducted a numerical investigation using CONVERGE software to analyze the impact of various piston bowl geometries on the performance and emissions of a gas/diesel RCCI engine operating at a medium load. The study utilized three distinct piston bowl geometries—the cylindrical, stock design, and bathtub-shaped bowl—while maintaining a fixed compression ratio (CR) of 16.1:1. A double injection strategy was employed to inspect the depth of the piston bowl, the existence of a beveled ring-land, and the engine speed on the RCCI engine's performance. The finding revealed that the piston bowl shape at low speeds has no impact on the combustion of the RCCI engine, but it has a considerable impact at high engine speeds. Increasing the engine speed caused a reduction in in-cylinder temperature and pressure, which in turn resulted in a delay in combustion phasing. As a result, both the ringing intensity (RI) and the gross indicated efficiency (GIE) decreased, while emissions of CO and UHC increased. The optimum piston bowl shape is the bathtub-shaped design since it provides the best engine performance and lowers emissions at high speeds. Moreover, increasing the depth of the

piston bowl to 1 mm or utilizing a chamfered ring-land by increasing the chamfer size up to 3 mm can increase the gross indicated efficiency (GIE) and minimize both CO and UHC emissions [29]. Wang et al. conducted a study on optimizing the geometry of the engine's combustion chamber by utilizing the NSGA-II with a kriging-based meta-model for a natural gas/diesel RCCI engine. The results showed that the indicative efficiency and NOx emissions were slightly improved, and CO and HC emissions were reduced by 33.55% and 56.4%, respectively [30]. In their study, Liu et al. optimized the diesel injection and operating parameters of a natural gas/diesel engine using the NSGA-II algorithm. The aim of this study was to minimize indicated specific fuel consumption (ISFC) and emissions of NOx and CH_4. The soot emission outcome meets the EURO VI emission standard. However, only some solutions fully comply with the EURO V NOx emission standard [31]. Shirvani et al. investigated the optimization of injection strategies for gasoline and diesel engines to minimize exergy destruction, maximize exergy efficiency, and reduce the noise index. An artificial neural network and the NSGA-II algorithm were employed to investigate optimal solutions. Exergy efficiency increases by up to 2%, and exergy destruction is reduced by approximately 2.3% compared with the base case. Reductions in soot and NOx emissions of 35% and 40%, respectively, were achieved [32]. Moradi et al. conducted an optimization study to determine the impacts of fuel rates, EGR, and SOI on the gasoline/diesel RCCI engine by applying the NSGAII algorithm. They found an enhancement of indicative and second-low efficiencies of 1.56% and 1.25%, respectively, along with a 16.67% reduction in NOx concentration [33].

Table 1. Methane and n-Heptane physio-chemical properties [19].

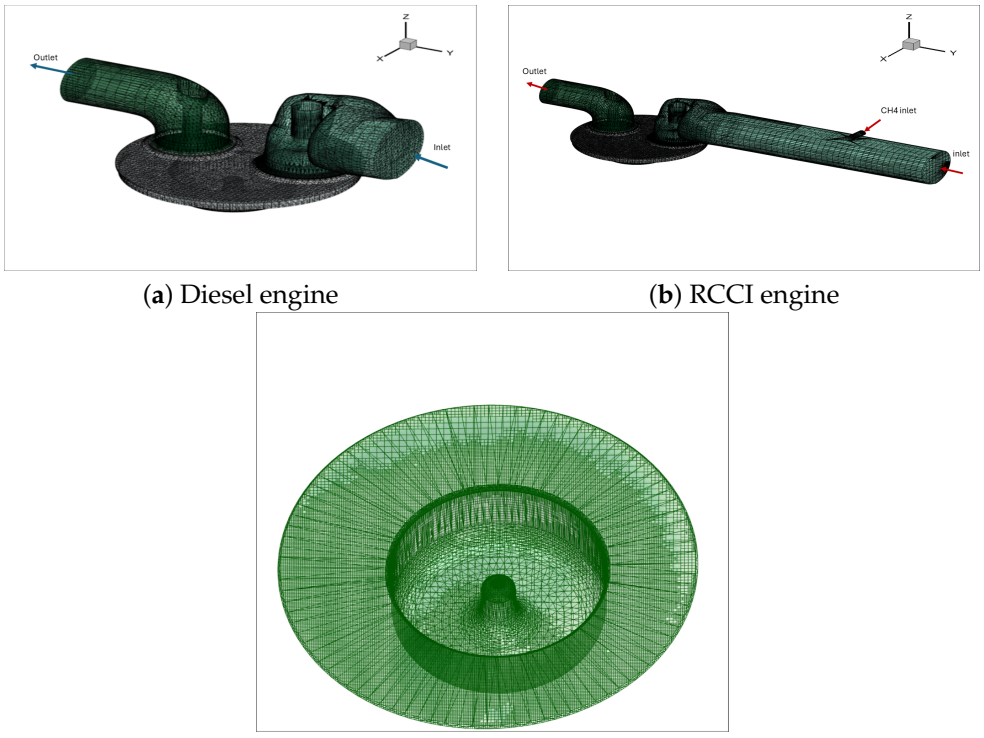
Properties	n-Heptane	Methane
Chemical formula	C_7H_{16}	CH_4
Density at 15 °C (g/m^3)	0.688	0.664
Lower heating value (MJ/kg)	44.24	49.94
Auto-ignition temperature (K)	558	810
Molecular weight	100.21	16.042
Cetane number	56	-
Octane number	-	130
Boiling point (K)	372	111.55

The objective of this study is to evaluate the impact of various operational parameters of a modified light-duty single-cylinder methane/diesel engine, including engine rotational speed (rpm), methane mass, diesel mass, the SOI, and the duration of diesel injection on indicated specific fuel consumption (ISFC), PFP, and emissions. The characteristics of the base engine are presented in Table 2, and the diesel and the RCCI engine models of this engine, in addition to the piston bowl shape, are shown in Figure 1. The sensitivity to the operational parameters is investigated to determine the most appropriate one in different circumstances. The non-dominated sorting algorithm NSGA II is used for the optimization study and to minimize ISFC simultaneously with decreasing tailpipe emissions. The research analyzing the variables that affect the combustion in RCCI engine, including the amount, timing, and duration for both premixed fuel, as well as direct injection fuel in addition to the effect of the engine rotation, is inadequate. The primary goal of this study is the extensive optimization of performance and tailpipe emissions, in comparison to the baseline conventional diesel engine, across a wide range of engine loads. Studying the effect of all the variables mentioned above and exploring the range of RCCI loads and on which excess air ratios methane/diesel light-duty engine work is a new gap that has been examined to recognize the main variable parameters that control RCCI mode to cope with the essential difficulties facing RCCI combustion, which is the second consequence of

this study. Finally, a sensitivity analysis is carried out to assess how the decision variables independently affect the objective functions, assisting in discovering the key variables affecting RCCI combustion. Moreover, this work is carried out to prepare and check the validity of our calculation methodology for the future H_2–diesel combustion study.

Table 2. Conventional diesel engine Antor LD 510 specifications.

Specification	Value
Cylinder volume (cc)	510
Compression ratio (CR)	17.5:1
Bore diameter/stroke (mm)	85/90
Number of valves	2
RPM	3000
IVO/IVC (°CA)	339/592
EVO/EVC (°CA)	135/388
Torque at rated speed (Nm)	25
Power (kW)	7.88
Injector hole diameter (mm)	0.29
Number of injector holes	4



(**a**) Diesel engine (**b**) RCCI engine

(**c**) Piston bowl shape

Figure 1. Diesel engine, piston bowl shape, and RCCI engine.

2. Numerical Methodology

2.1. Governing Equations

The following transport equations represent the dynamics of fluid flow, encompassing mass, momentum, energy conservation, and the transport of species [34].

$$\frac{\partial \rho}{\partial t} + \frac{\partial}{\partial x_k}(\rho u_k) = S \tag{1}$$

$$\frac{\partial (\rho u_i)}{\partial t} + \frac{\partial (\rho u_i u_j)}{\partial x_j} = \frac{\partial \sigma_{ij}}{\partial x_i} + S_i \tag{2}$$

where σ_{ij} represents the viscous stress tensor, and e_{ij} is the strain rate tensor.

$$\sigma_{ij} = -\left(p + \frac{2}{3}\mu\nabla \cdot u\right)\delta_{ij} + 2\mu e_{ij} \tag{3}$$

$$e_{ij} = \frac{1}{2}\left(\frac{\partial u_i}{\partial x_j} + \frac{\partial u_j}{\partial x_i}\right) \tag{4}$$

$$\begin{aligned}\frac{\partial}{\partial t}\left(\rho\left(e + \frac{1}{2}u_k^2\right)\right) + \frac{\partial}{\partial x_j}\left(\rho u_j\left(e + \frac{1}{2}u_k^2\right)\right) \\ = -\frac{\partial}{\partial x_j}(u_j p) + \frac{\partial}{\partial x_j}(u_i\sigma_{ij}) + \frac{\partial}{\partial x_j}\left(K\frac{\partial T}{\partial x_j}\right) \\ + \frac{\partial}{\partial x_j}\left(\rho\sum_m D_m h_m \frac{\partial Y_m}{\partial x_j}\right) + S\end{aligned} \tag{5}$$

$$\frac{\partial \rho_m}{\partial t} + \frac{\partial \rho_m u_j}{\partial x_j} = \frac{\partial}{\partial x_j}\left(\rho D_m \frac{\partial Y_m}{\partial x_j}\right) + S_m \tag{6}$$

$$\rho_m = Y_m \rho \tag{7}$$

where u represents the velocity, ρ is the density, ρ_m denotes the density of species m, and Y_m is the mass fraction of species m. D_m refers to the molecular mass diffusion coefficient for species m, while S_m is the corresponding source term. Additionally, h_m indicates the species-specific enthalpy, e is the specific internal energy, K stands for thermal conductivity, and $\frac{1}{2}u_k^2$ represents the kinetic energy term. Moreover, P denotes pressure, μ is the viscosity, and δ_{ij} is the Kronecker delta.

2.2. CFD Models

CONVERGE 3.0 CFD commercial software is used to solve numerically, mass, density-based Navier–Stokes equations, energy, and species equations for conventional diesel engine CDC and RCCI engine [34]. The in-cylinder turbulent flow is predicted using the Reynolds-averaged Navier–Stokes (RANS) equations in conjunction with the average generalized re-normalization group (RNG) turbulence model [35]. The automated cut-cell Cartesian grid approach automatically generates meshes and orthogonal mesh with hexahedrons. The mesh is updated at each timestep for movable boundaries. Adaptive mesh refinement (AMR) is employed to adjust the mesh resolution according to the varying conditions of the moving fluid, including factors such as velocity, temperature, species, scalars, passive variables, and boundary conditions, ensuring convergence. Furthermore, fixed embedding is applied to refine the mesh at specific critical locations, including cylinders, nozzles, and the fuel spray region, thereby allowing the coarse grid to accelerate the numerical solution in other regions [36]. The modified Pressure Implicit with the Splitting of the Operator (PISO) is utilized to solve the transport equations [37]. In this study, the Euler–Lagrangian method was employed. The Lagrangian method was employed to trace the movement of each droplet within the flow field. Meanwhile, the Eulerian method was applied to model the gaseous phase. The fuel parcels are introduced into the cylinder at a specific rate. The parcels are used to predict an identical group of drops. During the injection period, these droplets undergo various processes that promote their vaporization. The fuel particles may become unstable due to the forces exerted on their surfaces as they move through the gaseous medium within the cylinder. A breakup model is employed to solve this problem. The hybrid Kelvin–Helmholtz–Rayleigh–Taylor (KH-RT) model is employed to forecast the behavior of droplet breakup [38], and it is preferable since it is used in many other similar studies [39–41]. A detailed chemical model, SAGE,

is utilized to simulate the combustion process [42]. The reduced primary reference fuel (PRF) mechanism is employed to predict the n-heptane and methane chemical reactions, composed of 464 reactions and 76 species [43]. For simplicity, n-heptane (C7H16) is used as a substitute for diesel fuel because of its analogous cetane number. The Frossling model was selected to simulate the droplet evaporation process [44]. For spray drop coalescence, the post-collision outcome model is used [45], and the No Time Counter (NTC) method is applied to model drop collision [46]. The Rebound/slide model is used to simulate the spray droplets' interaction with solid surfaces [47]. The extended Zeldovich mechanism is utilized to find the amount of NO formation [48]. The empirical model of Hiroyasu–NSC is used to predict soot oxidation [49]. CONVERGE 3.0 CFD calculated the species, including CO, CO2, methane slip (CH_4), and UHC, by solving transport equations with the help of the SAGE combustion model and reaction mechanism. Table 3 provides a concise overview of the sub-models employed in the simulation. These models are extensively used in other studies [50–52].

Table 3. Processes and their corresponding models.

Process	Model
Turbulence	RANS and RNG k-ε
Combustion	SAGE
Drop collision	NTC method
Break-up process of diesel spray	Kelvin–Helmholtz and Rayleigh–Taylor (KH-RT)
Evaporation of droplets	Frossling model
Droplet coalescence	Post-collision outcome model
Spray droplet interaction with solid surfaces	Rebound/slide model
Formation of NO_x	Zeldovich mechanism
Soot oxidation rate	Hiroyasu–NSC empirical soot model

2.3. Optimization Approach

In this study, the modeFRONTIER 2024R1.1 software is utilized to implement the Non-Dominated Sorting Genetic Algorithm (NSGA) II in conjunction with CONVERGE 3.0 CFD to optimize the operational factors of the methane/diesel RCCI engine [53]. NSGA II is considered a robust optimization design of experiments algorithm, and robustness means the capability of the optimization algorithm to gain the maximum or minimum value of the maximized or minimized objective functions, respectively, even if the starting point is different from the final solution. The implemented optimizing algorithm in mode FRONTIER needs to be initialized by random or specified experimental designs (DOE). Equation (8) shows the minimum DOE size.

$$\text{Number of designs} = 2 \times M \times B \tag{8}$$

where M and B are the number of input variables and objectives, respectively.

Figure 2 illustrates the flowchart of the NSGA II algorithm, and the basic steps to implement this algorithm are as follows [54]. Before executing the selection, the citizens are ranked based on the degree of nondomination of each member. First, the non-dominant members are identified as the current citizens. Then, all these members are deemed to compose the first nondominated front within the citizens and are given a high dummy fitness amount. To preserve variety among the citizens, these labeled citizens are then distributed along with their values of dummy fitness. Sharing is attained by employing a selection process depending on weakened fitness amounts, where each citizen's original fitness amount is divided by a factor relevant to the number of nearby citizens, leading to several optimal points for the citizens. After that, the nondominated individuals are

disregarded temporarily to process the rest of the citizens similarly and classify candidates for the next nondominated front. These nondominated results are granted an updated dummy fitness value, which is kept less than the lower value of the shared dummy fitness value of the prior front. This process persists until all citizens are sorted into several fronts and arranged in descending order, where the first front has a higher fitness value, the second one has a lower one, and so on [55]. NSGA-II performs two operations to create new designs: mutation and crossover. Crossover comprises several designs in which the parent generation subrogates its genetic information to construct a new design for the following generation. The objective is to produce individuals with better traits than their parents while preserving the variety of the citizens. Mutation introduces random alterations to the genetic information of a design, generating a new variant in the subsequent generation. Doing so presents a degree of randomness in the search. It enables exploring various configuration space regions to prevent the optimization algorithm's early convergence. Crossover also assists in improving the convergence. The maximum probability for the crossover from other studies is around 0.6 to 0.95. In contrast, the mutation probability is significantly low in the range of 0.001 to 0.05, which can result in a high level of mixing and exploitation with comparatively minimal exploration [54]. In the present study, the peak firing pressure (PFP) and the indicated specific fuel consumption (ISFC) are selected as objectives of the optimization study. Meanwhile, CO, UHC, and NOx emissions are selected as the constraints. Five independent operational parameter variables were optimized simultaneously, including rpm, diesel fuel mass, methane mass, SOI, and the duration of diesel fuel, in addition to two dependent variables of nitrogen (N_2) and oxygen (O_2) percentages.

For the present work, the operational parameters, objectives, and constraints are shown in Table 4. For the optimization study, the simulation was run from the intake valve closed IVC to the exhaust valve open EVO for the entire cylinder; since the piston bowl is non-axisymmetric, the amount of N_2 and O_2 that represents air inside the cylinder will be mixed with premixed fuel, which is the methane in this study under specific conditions; these gases represent 1% when initializing the cylinder region in the CFD model. The following equations show objectives, constraints, and the dependent and independent variables initialized in the cylinder.

$$P_{CH_4} + P_{N_2} + P_{O_2} = 1 \tag{9}$$

$$P_{O_2} = (1 - P_{CH_4}) \times 0.233 \tag{10}$$

$$P_{N_2} = (1 - P_{CH_4}) \times 0.767 \tag{11}$$

where P_{CH_4} is the independent variable that represents the percentage of methane initialized in the cylinder, which varies according to the algorithm. P_{N_2} and P_{O_2} are the variables that are dependent on P_{CH_4}, representing the percentage of nitrogen and oxygen initialized in the cylinder.

$$CO = \frac{\left(\frac{m_{CO}}{h}\right)(\text{g/h})}{P(\text{kW})} \tag{12}$$

$$HC = \frac{\left(\frac{m_{HC}}{h}\right)(\text{g/h})}{P(\text{kW})} \tag{13}$$

$$NO_x = \frac{\left(\frac{m_{NO_x}}{h}\right)(\text{g/h})}{P(\text{kW})} \tag{14}$$

$$ISFC = \frac{\left(\frac{(m_{CH_4} + m_d)}{h}\right)(\text{g/h})}{P(\text{kW})} \tag{15}$$

where m_{CO}, m_{HC}, m_{NO_x}, m_{CH_4}, and m_d are the quantities of CO, HC, NO_x, CH_4, and diesel, respectively, at EVO, and P is the power.

$$\lambda = \phi^{-1} = \frac{\sum_j \sum_i N_i \eta_{O,i}}{\sum_j 2 \sum_i N_i \eta_{C,i} + \frac{1}{2} \sum_i N_i \eta_{H,i}} \quad (16)$$

where N_i denotes the mole number of species i, while j represents the total number of cells in the field. Additionally, $\eta_{O,i}$, $\eta_{H,i}$, and $\eta_{C,i}$ correspond to the number of oxygen (O), hydrogen (H), and carbon (C) atoms, respectively, for species i.

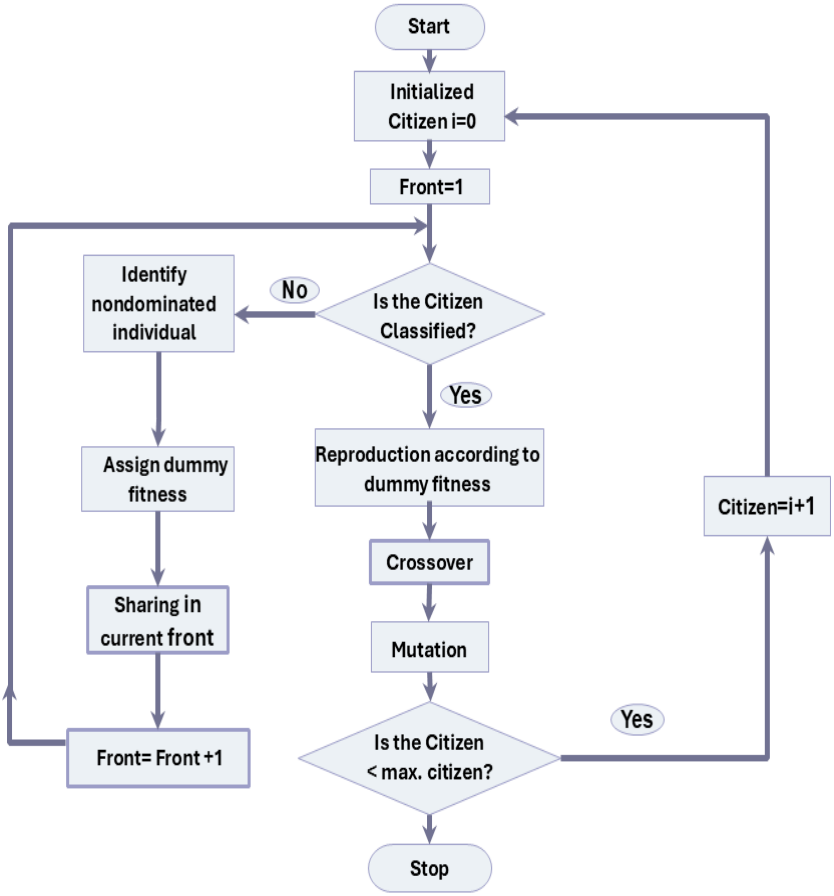


Figure 2. The flowchart of NSGA II.

Table 4. The operational parameters, objectives, and constraints used for the optimization study.

Operational Parameter	Range	Objective	Constraint	Range
Rotational velocity (rpm)	2000–3250	Minimize PFP (MPa)	HC	<0.13 g/kWh
Premixed CH_4 fraction	0.02–0.026	Minimize ISFC	NOx	<2 g/kWh
Diesel mass (mg)	1.4–7	-	CO	<1.5 g/kWh
SOI (°CA)	−35 to −10	-	-	-
Diesel injection duration (°CA)	1.5–6	-	-	-

2.4. Validation Study

The original conventional diesel engine (CDE) was modeled as a whole engine using experimental data for initial boundaries, including 21.206 mg/stroke of diesel fuel, SOI of −26 CA aTDC, and diesel fuel pressure of 180 bars. The experimental data for the diesel engine case were provided by the Anadolu company. Then, the model was run for three consecutive cycles to wash out the initial boundary conditions and to predict accurate

results. Three mesh sizes were used for the mesh-independent study of CONVERGE 3.0 CFD: coarse mesh of 8 mm, medium mesh of 4 mm, and fine mesh of 3 mm. A 4 mm mesh size gives accurate results, just as a fine mesh does. Therefore, a 4 mm mesh size was employed in this study to balance prediction accuracy and computational cost, as illustrated in Figure 3. The in-cylinder pressure results for the diesel engine for both CONVERGE 3.0 CFD and experiment were validated against each other, as presented in Figure 4a. The in-cylinder pressure of the models and tests had adequate harmonization; in addition, there was a slight variation in NOx emissions results between the simulation and the experiment, which was 2% less, which proves that the CFD models were successfully calibrated. Additionally, the RCCI engine simulation results were validated using experimental data from published journal articles, specifically by comparing in-cylinder pressure and heat release rate, as shown in Figure 4b [56]. This validation further demonstrates that the CFD model was well calibrated. So, this model was used as the basis of the methane/diesel model. Various quantities of methane and diesel were introduced into the engine, with methane supplied through the intake port via inlet boundary conditions, while diesel was directly injected into the cylinder. The model was run for three continuous cycles, and the boundary conditions of the third cycle at IVC was used as the initial conditions for the closed cycle of the hole engine. Here, the whole engine without ports was used for the optimization since the piston bowl of the cylinder is non-axisymmetric. The boundary conditions applied for the closed cycle used in the optimization study are presented in Table 5.

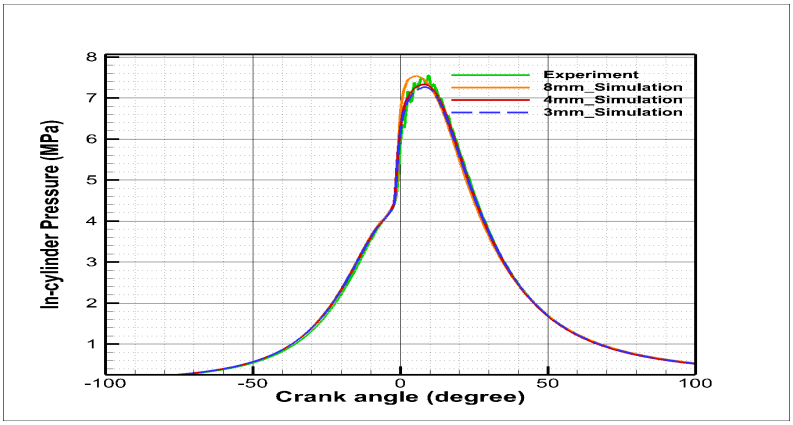
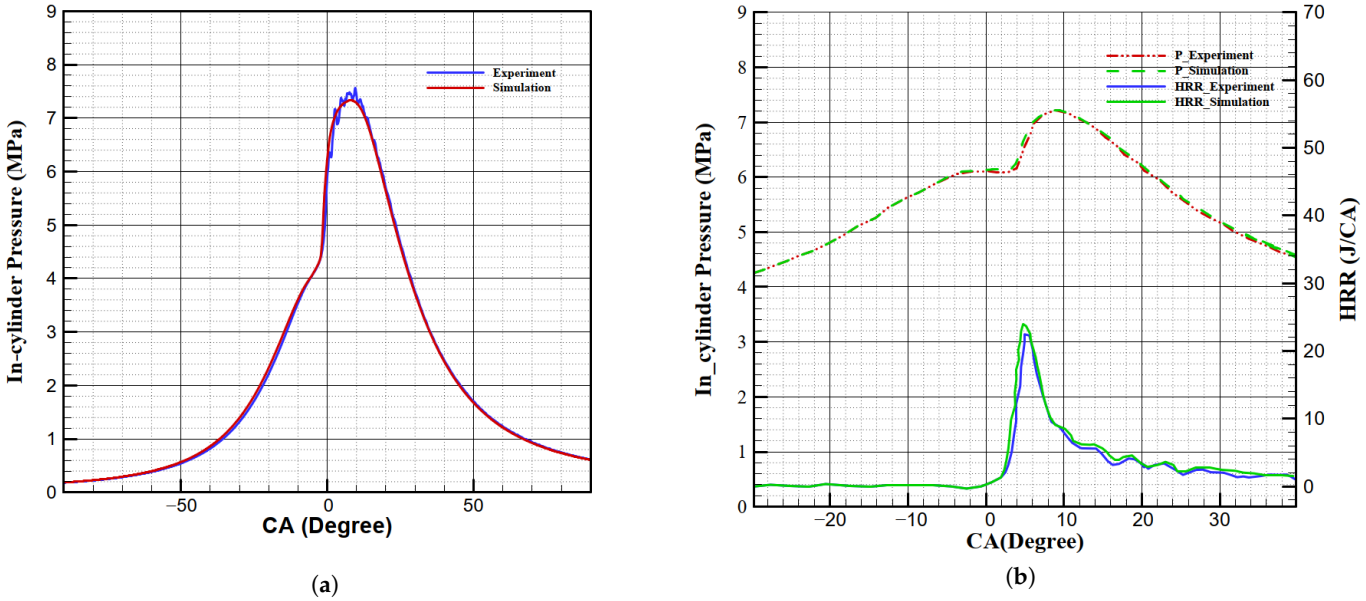


Figure 3. In-cylinder pressure for mesh independence study.

Table 5. Initial conditions for a closed cycle.

Parameter	Value
Swirl ratio	2.57
Turbulent kinetic energy (m^2/s^2)	61.2
Energy dissipation (m^2/s^3)	43,512.2
Pressure (Pa)	116,545.7
Temperature (K)	400.8
Start of injection SOI (CA aTDC)	−23
Diesel mass (mg)	1.5
Diesel injected pressure (bar)	180
Methane mass (mg)	9.31



(**a**) (**b**)

Figure 4. Validation study of the simulation and experimental results for diesel and RCCI engines. (**a**) Validation of the in-cylinder pressure of the diesel engine; (**b**) validation of the in-cylinder pressure and the HRR of RCCI engine [56].

3. Results

This section explores the optimization of operational strategies and examines the impact of varying quantities of low-reactivity and high-reactivity fuels under different loads and rpm on a light-duty RCCI engine using an extensive data pool generated by the NSGAII algorithm. The data pool is sorted into three main groups: feasible outcomes, which meet the objectives and constraints; infeasible outcomes, which do not meet any objective or constraints; and Pareto outcomes. The optimization runs 207 design evolutions; 76 designs are feasible, and 33 are the Pareto results. As noticed in Figure 5, the feasible solutions are diminished at high loads, which indicates a colossal optimization challenge. These outcomes address the obstacles to implementing the discernible barriers at varied rpm, fuel quantities, SOI, and duration and their influence on the optimization approach.

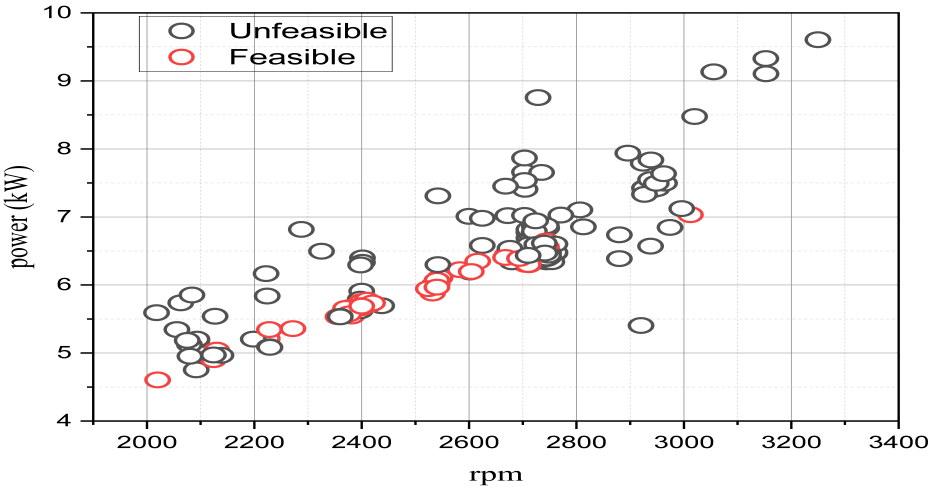
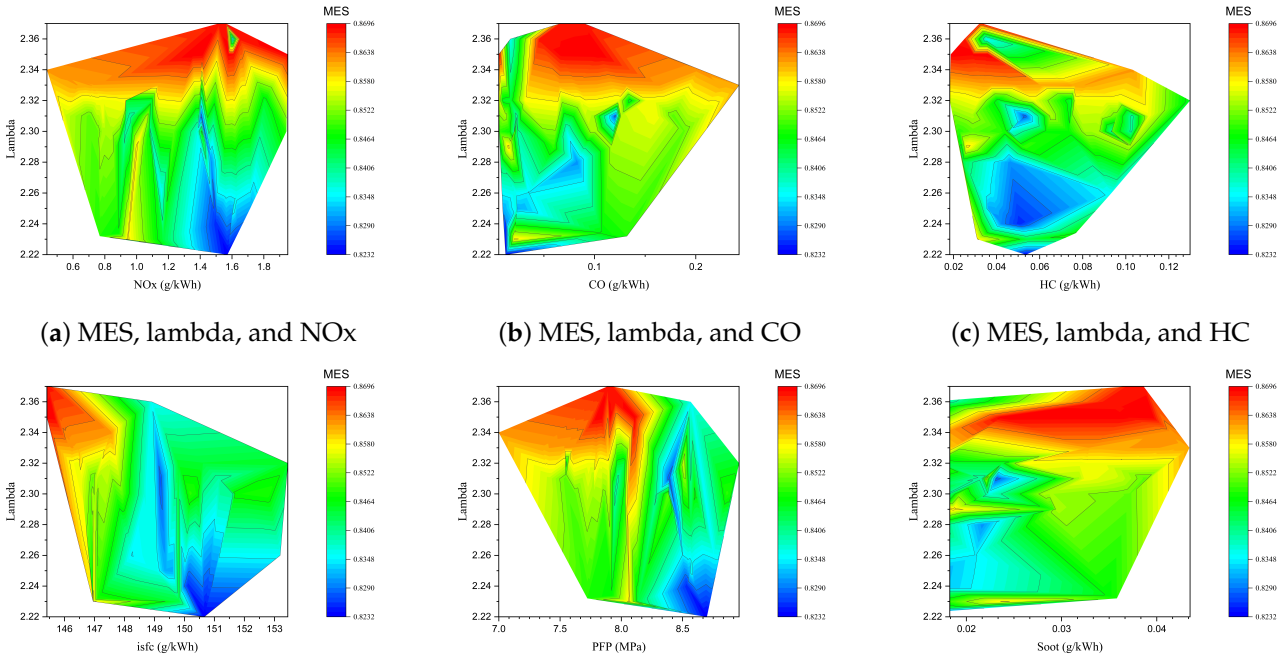


Figure 5. Power vs. rpm.

3.1. Lambda and MES Impacts

For clarity, feasible outcomes are used for graphs in this part. Figure 6 depicts the impact of methane energy share (MES) and the excess air ratio on the performance and emissions characteristics of the RCCI engine. It is noticed that all feasible results are in the lambda range of 2.22 to 2.37, and MES in the range of 82 to 87 %. The best NOx results are at a lambda of 2.34 and an MES of 86%. The best CO emission outcome is between 2.29 to 2.35 and at an MES above 84%, while the best HC emissions results are in the lambda range of 2.32 to 2.35 and at an MES above 85.4%. The optimum outcome of ISFC is encountered at a high lambda range of 2.35 to 2.37 and an MES above 86.3%. All feasible outcomes are within a range of PFP from 7 to 9 MPa.



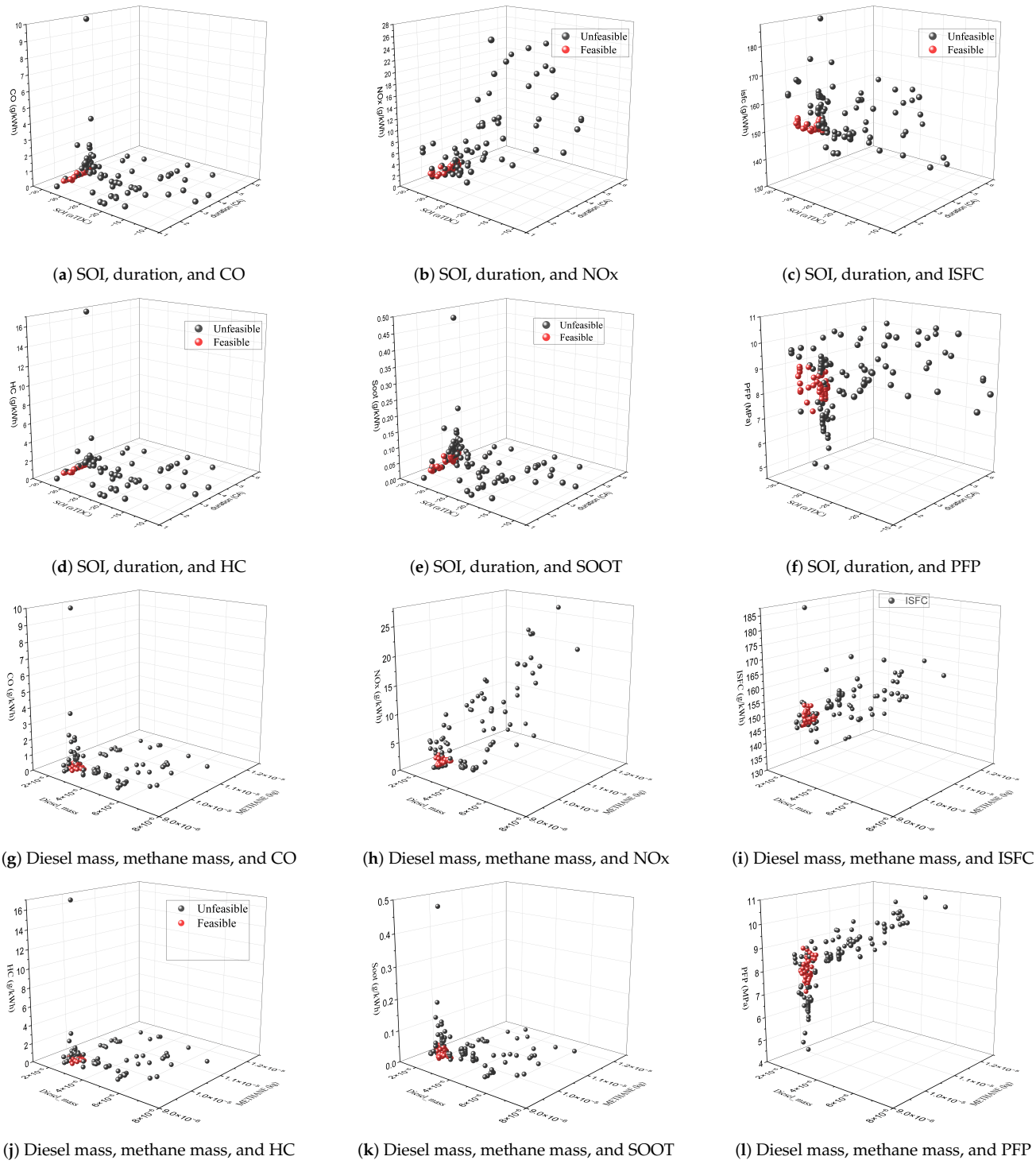
(**a**) MES, lambda, and NOx (**b**) MES, lambda, and CO (**c**) MES, lambda, and HC

(**d**) MES, lambda, and ISFC (**e**) MES, lambda, and PFP (**f**) MES, lambda, and soot

Figure 6. Contour plots of the MES and Lambda impacts on emissions, PFP, and ISFC.

3.2. Operational Parameters Impact

This part will discuss the effects of operational parameters. As shown in Figure 5, the amount of power is linearly proportional with increasing rpm, and the maximum ratio between RCCI engine power and diesel engine design power is 89.5%. Moreover, it shows feasible results in the 2020 to 3010 rpm range. However, there is no feasible solution in the 2800 to 3010 rpm range. The impacts of SOI, injection duration, methane mass, and diesel mass are shown in Figure 7, which shows that as the SOI retarded to near TDC, CO and UHC emissions increased, while all feasible results were obtained within the start of injection (SOI) range of (−35 to −34) CA aTDC. Moreover, the duration of the injected diesel fuel affects the performance and emissions of the RCCI engine, and it also influences the injected fuel pressure; a longer injection duration results in lower diesel fuel pressure, whereas a shorter injection duration leads to higher diesel fuel pressure. Moreover, it is found that the feasible results are in the diesel injection duration range of 2 to 3.56 CA.



(**a**) SOI, duration, and CO (**b**) SOI, duration, and NOx (**c**) SOI, duration, and ISFC

(**d**) SOI, duration, and HC (**e**) SOI, duration, and SOOT (**f**) SOI, duration, and PFP

(**g**) Diesel mass, methane mass, and CO (**h**) Diesel mass, methane mass, and NOx (**i**) Diesel mass, methane mass, and ISFC

(**j**) Diesel mass, methane mass, and HC (**k**) Diesel mass, methane mass, and SOOT (**l**) Diesel mass, methane mass, and PFP

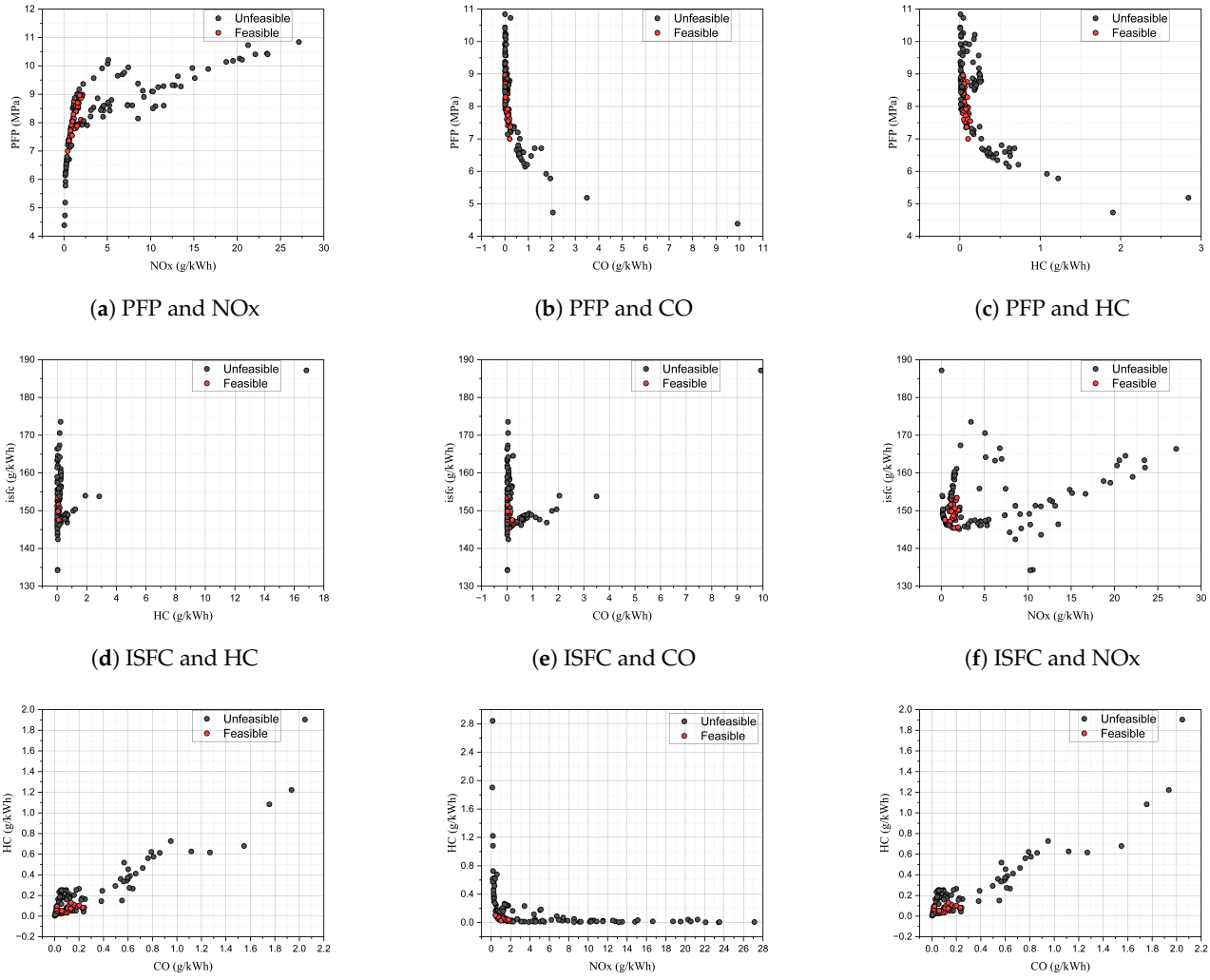
Figure 7. Three-dimensional scatter plot for the effect of operational parameters on ISFC and emissions.

3.3. Emissions Results

Figure 8 exhibits all populations and the Pareto front for the optimization process. According to this figure, the evolution evolves toward decreasing the objective and constraint values of ISFC, PFP objectives, and CO, NOx, and UHC constraints. CO emissions originate from incomplete combustion caused by insufficient oxygen in the combustion chamber. The homogeneity of the air–fuel mixture within the combustion chamber is considered another key factor influencing CO emissions. In some situations, even though oxygen is sufficient in the combustion chamber, a lack of mixture homogeneity leads to rich regions,

resulting in higher CO emissions. Increasing the quantity of diesel fuel might increase the CO emissions due to the deficit of the in-cylinder dynamics in controlling the homogeneous mixing of air/fuel in the cylinder. Additionally, CO emissions may rise as a result of the low-temperature combustion characteristics of the RCCI engine. Meanwhile, UHC emissions primarily result from bulk quenching, wall quenching, and lower combustion temperatures within the combustion chamber. Furthermore, the presence of non-uniform regions within the cylinder can lead to the formation of hydrocarbons (HCs). As seen from row 1 in Figure 8, most infeasible solutions happened in the range of PFP < 7 MPa and PFP > 9 MPa. This happens at lower PFP due to incomplete combustion since the UHC and CO emissions results are out of the acceptable range of optimization constraints, while infeasible solutions happen at higher PFP mostly because of the NOx emissions being out of the range due to high temperature. Figure 8, row 2 shows the influence of each UHC, CO, and NOx emission on IFSC. It seems that both UHC and CO follow approximately the same pattern as ISFC, starting from high and low values of ISFC; all outcomes are infeasible, which might be because of high NOx emissions while at ISFC in the feasible range, an infeasible outcome due to the combined effect of NOx, CO, and UHC emissions. Figure 8, row 3, shows the Pareto outcomes between HC and CO, which have a nearly linear relationship. In contrast, both UHC and CO emissions show a trade-off relationship with nitrogen oxide (NOx) emissions. This study will briefly discuss elective optimum cases, where case (A) shows the optimum case that emits the lowest UHC and CO emissions and gives the lowest ISFC; case (B) is the optimum case that emits less NOx; case c is the optimum result of soot; and case D is the optimum case in terms of power. It can be noticed that all cases were at an SOI of −35 aTDC, except case D, which was at −34 aTDC, which means these values are the optimum values for SOI.

In case A, the high temperature is settled for a longer duration in the cylinder, which is why the CO and UHC emissions and ISFC have the lowest values because of enhanced combustion. For this case, the SOC, CA 50, and CD are (−0.919, 3.03), CA aTDC, and 8.739 CA, respectively, with noting that the CA10 is defined as the start of combustion (SOC). This case gives the lowest power of 5.36kW and a higher IE of 51% and utilizes less diesel fuel at 1.71 mg injected at a pressure of 150 bars at 2270 rpm. The high-temperature range in case B is lower than in the other cases. It settles within a short time in the chamber, which is why the NOx emissions in this case are less than in other cases, even though all cases are considered optimum cases of this study. The emissions in case B are within the EURO VI standards. Moreover, the start of combustion (SOC) is at 2.56 CA aTDC, the CA 50 is retarded to 8.25 CA aTDC, and the combustion duration is 9.74 CA. This case gives a power of 5.97 kW, an IE of 50%, and a utilized diesel fuel of 1.82 mg injected at a pressure of 272.3 bars at 2540 rpm. Case C emits lower soot emissions because it has the most prolonged combustion duration at 8.078 CA. Also, it has the most advanced SOC at −2.45 compared with other cases since expediting the SOC in the RCCI engine mitigates soot emissions by enhancing premixed combustion. In contrast, when SOC is retarded, soot emissions will increase owing to fuel-rich localized zones. Moreover, the peak heat-release value is greater than in the other cases, resulting in the highest PFP and peak temperature. The CA 50 is 3.33 CA aTDC. This case produced a power of 6.35 kW and an IE of 49% and utilized a higher quantity of diesel fuel, 2.44 mg, injected at a pressure of 365.4 bars at 2620 rpm. Case D produces the highest power at 7.03 kW, indicating that the most suitable power should be less than 0.89 from the maximum allowable design load of the original diesel engine, primarily due to the high NOx emissions at higher loads. For this case, the SOC, CA 50, and CD are (−1.78, 5.72), CA aTDC, and 11.38 CA, respectively. The IE was 49% and used less diesel fuel, at 2.06 mg injected at a pressure of 496 bars and at 3010 rpm, as shown in Figures 9–11.

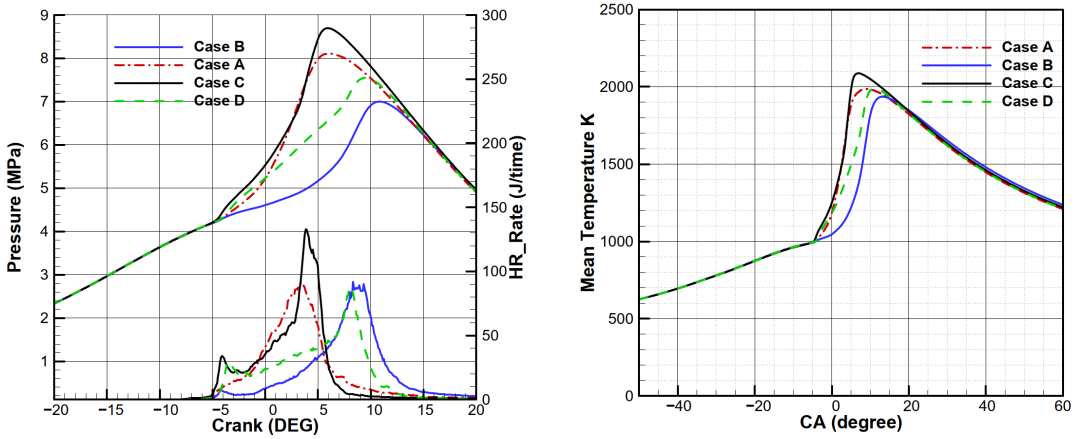


(**a**) PFP and NOx (**b**) PFP and CO (**c**) PFP and HC

(**d**) ISFC and HC (**e**) ISFC and CO (**f**) ISFC and NOx

(**g**) HC and CO (**h**) HC and NOx (**i**) CO and NOx

Figure 8. Scatter plot for objectives and constraints.



(**a**) In-cylinder pressure and HRR (**b**) In-cylinder temperature

Figure 9. In-cylinder pressure, HRR, and temperature for selected optimum cases.

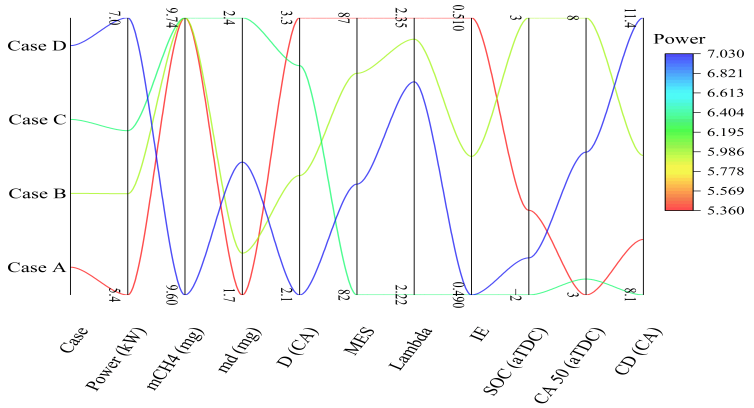
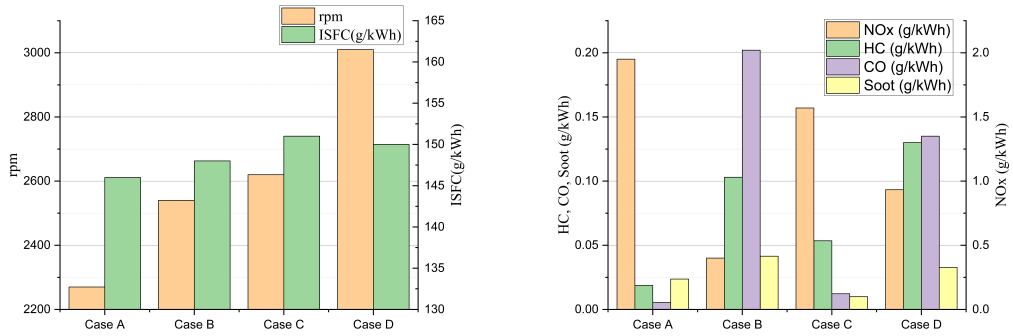


Figure 10. Parallel plot power, CH_4 mass, diesel mass, duration (D), MES, Lambda, IE, SOC, CA50, and CD for all selected optimum cases.



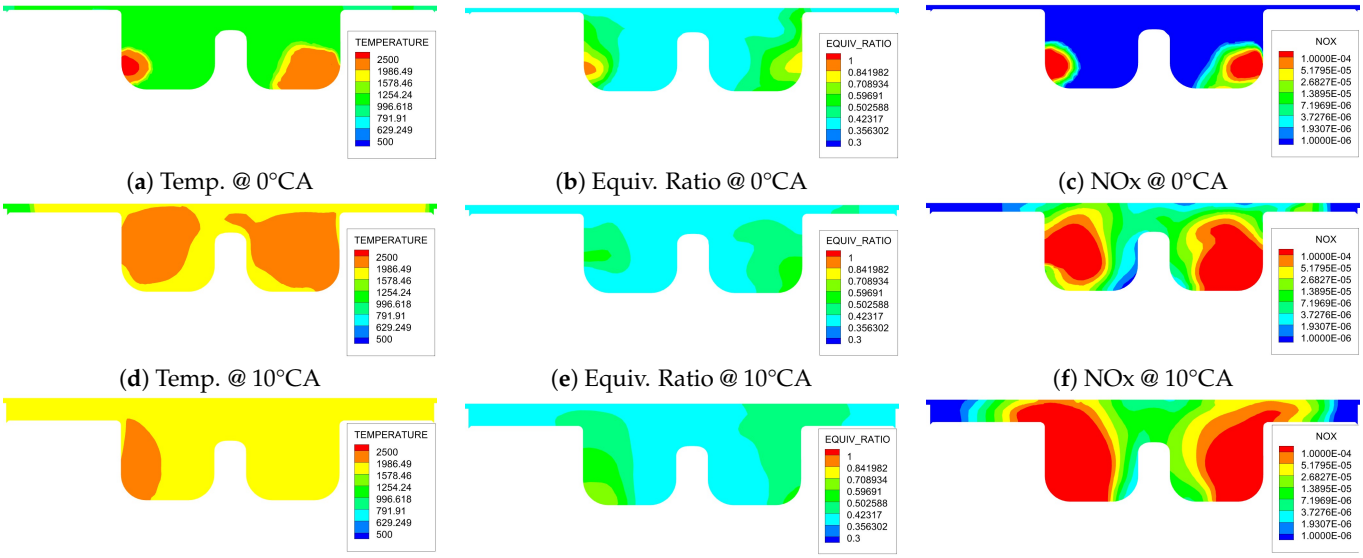
(**a**) ISFC and rpm for optimum cases (**b**) HC, CO, and NOx for optimum cases

Figure 11. Comparison figure for ISFC and rpm, and HC, CO, and NOx emissions for selected optimum cases.

The tradeoff results between NOx with UHC and CO emissions can be interpreted physically. As seen in Figure 12, for case A, the temperature is high near the wall in the piston bowl region due to rich fuel in this region, which is why the NOx in this case is higher, and due to the the lower HC and CO emissions due to the enhanced combustion characteristics. In contrast, in case B, the low combustion temperature can increase the UHC and CO due to incomplete combustion, mostly in the center of the combustion chamber, while NOx emissions can be emitted in the lower range primarily in the squish region, as shown in Figure 13. Table 6 presents a comparison of emissions and performance outcomes based on data collected from the literature. This study achieves advanced IE and lower UHC and CO emissions, in addition to comparable results for soot and NOx, which are better than those of some studies.

Table 6. A comparison of the results for the present study with the literature's results.

Reference	IE %	ISFC g/kWh	NOx g/kWh	UHC g/kWh	CO g/kWh	Soot g/kWh
[26]	48.7	-	0.57	0.8	0.2	0.085
[27]	-	-	0.07	6.2	22.1	-
[31]	-	205.6	1.66	-	-	0.01
[57]	48.8	170.8	0.11	2.6	4	0.0009
Present Study	50	148	0.4	0.202	0.103	0.04

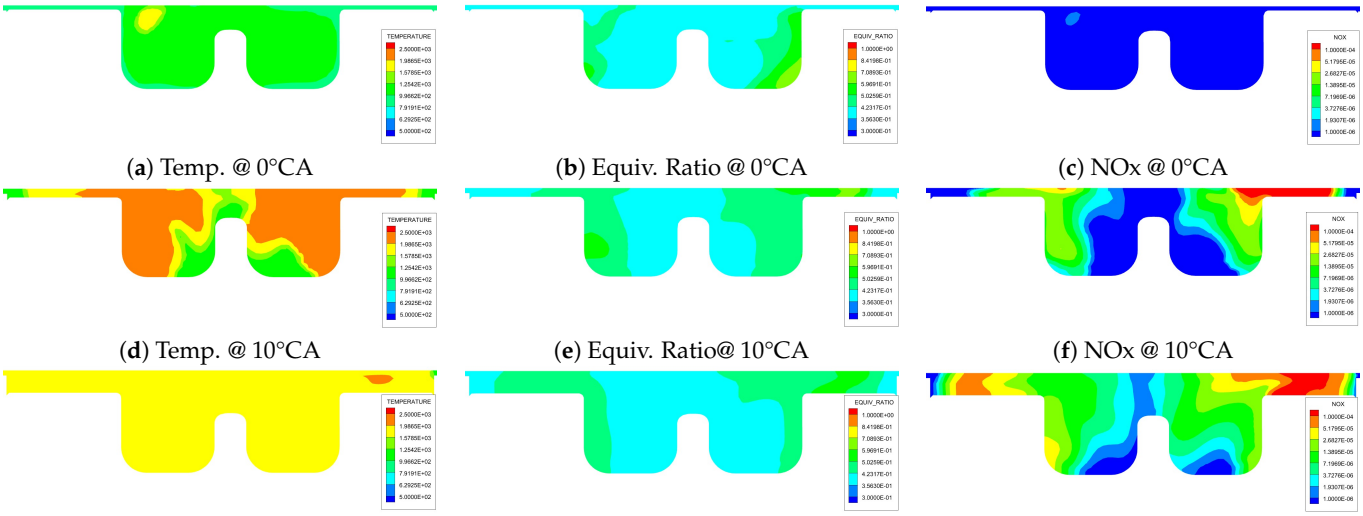


(**a**) Temp. @ 0°CA (**b**) Equiv. Ratio @ 0°CA (**c**) NOx @ 0°CA

(**d**) Temp. @ 10°CA (**e**) Equiv. Ratio @ 10°CA (**f**) NOx @ 10°CA

(**g**) Temp. @ 20°CA (**h**) Equiv. Ratio @ 20°CA (**i**) NOx @ 20°CA

Figure 12. Contour plot of in-cylinder temperature, equivalent ratio, and NOx emissions for case A.



(**a**) Temp. @ 0°CA (**b**) Equiv. Ratio @ 0°CA (**c**) NOx @ 0°CA

(**d**) Temp. @ 10°CA (**e**) Equiv. Ratio@ 10°CA (**f**) NOx @ 10°CA

(**g**) Temp. @ 20°CA (**h**) Equiv. Ratio @ 20°CA (**i**) NOx @ 20°CA

Figure 13. Contour plot of in-cylinder temperature, equivalent ratio, and NOx emissions for case B.

4. Conclusions

This paper presents an extensive optimization analysis of the impacts of diesel and methane masses, diesel injection duration, and engine rotational speed, which were optimized numerically by employing the NSGAII algorithm and CONVERGE 3.0 CFD via modeFRONTIER 2024R1.1 optimization software to obtain optimum cases regarding decreasing PFP, ISFC, and (CO, HC, NOx) emissions. The study ended with the main conclusions, summarized as follows.

- A well-justified selection of parameters, meshing strategies, and numerical methods ensures that simulations are both computationally feasible and practically useful.
- The highest indicative thermal efficiency of the methane/diesel RCCI engine was 51%, with an efficiency enhancement of 10% compared with the diesel engine.
- High power was achieved by RCCI engines, but with a tradeoff of high NOx emissions, which were out of standards, so the highest power achieved with an acceptable range of emissions and without being used after treatment was 7.03 kW, which is in the range of 0.89 from the maximum allowable load of CDE.

- All feasible results were in the range of the access air ratio of 2.22 to 2.37, MES in the range of 0.82 to 0.87, methane mass of 9.45 to 9.87 mg, diesel mass range of 1.71 to 2.44 mg, duration of 1.99 to 3.36 CA, SOI of −34 to 35 aTDC, and rotational speed range of 2020 to 3010 rpm.
- The minimum outcomes of (CO, HC) emissions and ISFC achieved were (0.00543, 0.0187) g/kWh and 146 g/kWh, respectively, which are lower than the CDE emissions by 99%, 72%, and 28.7%, respectively.
- Minimum NOx emissions were gained when the high range of cylinder temperature was the lowest and stayed for a short period. This was within the EURO IV standards of 0.4 g/kWh with a reduction of 97.5% compared with CDE.
- Minimum soot emissions were obtained when the SOC advanced and the in-cylinder temperature in the high range was higher than in other selected optimum cases.
- The improvement in IFSC along with reduced emissions suggests that utilizing methane-diesel in internal combustion engines is a cost-effective and promising approach.

Future Studies

This work will also direct us and show the validity of our computational methodology for a future H_2–diesel combustion study, which will be performed in a similar manner.

Author Contributions: A.H.S.A.: Methodology, Investigation, Visualization Software, Writing—original draft. M.Z.G.: Review & editing, Supervision, Methodology, Conceptualization. M.Y.: review and editing—original draft, Supervision, Software, Methodology, Conceptualization. All authors have read and agreed to the published version of the manuscript.

Funding: This research received no external funding.

Data Availability Statement: The original contributions presented in this study are included in the article. Further inquiries can be directed to the corresponding author.

Acknowledgments: The authors wish to acknowledge Anadolu Company for supplying experimental data. They would also like to express their gratitude to Convergent Science for providing free licenses of CONVERGE CFD and ESTECO software company for providing modeFRONTIER optimization software.

Conflicts of Interest: The authors declare no conflicts of interest.

Abbreviations

The following abbreviations are used in this manuscript:

AMR	Adaptive Mesh Refinement
ANN	Artificial Neural Network
aTDC	After Top Dead Center
BMEP	Brake Mean Effective Pressure
CA10	Crank Angle at 10% Mass Fraction Burned
CA50	Crank Angle at 50% Mass Fraction Burned
CA90	Crank Angle at 90% Mass Fraction Burned
CD	Duration of Combustion
CDE	Conventional Diesel Engine
CFD	Computational Fluid Dynamics
CO	Carbon Monoxide
CR	Compression Ratio
DOE	Experimental Design
EGR	Exhaust Gas Recirculation
EVO	Exhaust Valve Opening

HCCI	Homogeneous-Charge Compression Ignition
IMEP	Indicated Mean Effective Pressure
ISFC	Indicated Specific Fuel Consumption
IVC	Intake Valve Closure
LIVC	Late Intake Valve Closure
LTC	Low-Temperature Combustion
MES	Methane Energy Share
MN	Methane Number
NOx	Nitrogen Oxides
NSGA-II	Nondominated Sorting Genetic Algorithm-II
PFP	Peak Firing Pressure
PPCI	Partially Premixed Compression Ignition
RANS	Reynolds-Averaged Navier–Stokes Equations
RCCI	Reactivity-Controlled Compression Ignition
RI	Ringing Intensity
SCR	Selective Catalytic Reduction
SOC	Start of Combustion
SOI	Start of Injection
TDC	Top Dead Center
UHC	Unburned Hydrocarbons

References

1. Raimi, D.; Zhu, Y.; Newell, R.G.; Prest, B.C.; Bergman, A. Global energy outlook 2023: Sowing the seeds of an energy transition. *Resour. Future* **2023**, *1*, 1–44.
2. Yapıcı, E.Ö; Al-Attwani, A.H.S. Thermodynamic Analysis And Simulation of Steam Turbine Power Plant Hybrid With Parabolic Trough Collectors; A Study in Iraq. *Mugla J. Sci. Technol.* **2019**, *5*, 1–12.
3. European Environment Agency. *Transport and Environment Report 2022—Digitalisation in the Mobility System: Challenges and Opportunities*; (Issue 07); European Environment Agency: Copenhagen, Denmark, 2022. [CrossRef]
4. Milojević, S.; Savić, S.; Marić, D.; Stopka, O.; Krstić, B.; Stojanović, B. Correlation between emission and combustion characteristics with the compression ratio and fuel injection timing in tribologically optimized diesel engine. *Teh. Vjesn.* **2022**, *29*, 1210–1219.
5. Milojević, S.; Glišović, J.; Savić, S.; Bošković, G.; Bukvić, M.; Stojanović, B. Particulate matter emission and air pollution reduction by applying variable systems in tribologically optimized diesel engines for vehicles in road traffic. *Atmosphere* **2024**, *15*, 184. [CrossRef]
6. Kokjohn, S.L.; Hanson, R.M.; Splitter, D.A.; Reitz, R.D. Experiments and modeling of dual-fuel HCCI and PCCI combustion using in-cylinder fuel blending. *SAE Int. J. Engines* **2010**, *2*, 24–39.
7. SivaPrasad, K.; Rao, S.S.; Raju, V.R.K. Enhancement of mixture homogeneity for DI-CI engine to achieve Homogeneous Charge Compression Ignition (HCCI) combustion characteristics: A numerical approach. *Energy Sources Part A Recovery Util. Environ. Eff.* **2022**, *44*, 4318–4333.
8. Pandey, S.; Diwan, P.; Sahoo, P.K.; Thipse, S.S. A review of combustion control strategies in diesel HCCI engines. *Biofuels* **2018**, *9*, 61–74.
9. Noehre, C.; Andersson, M.; Johansson, B.; Hultqvist, A. *Characterization of Partially Premixed Combustion*; SAE Technical Paper No. 2006-01-3412; SAE International: Warrendale, PA, USA, 2006.
10. Manente, V.; Johansson, B.; Tunestal, P. *Partially Premixed Combustion at High Load Using Gasoline and Ethanol, a Comparison with Diesel*; SAE Technical Paper No. 2009-01-0944; SAE International: Warrendale, PA, USA, 2009.
11. Hanson, R.M.; Kokjohn, S.L.; Splitter, D.A.; Reitz, R.D. An experimental investigation of fuel reactivity controlled PCCI combustion in a heavy-duty engine. *SAE Int. J. Engines* **2010**, *3*, 700–716.
12. Dempsey, A.B.; Walker, N.R.; Reitz, R. Effect of piston bowl geometry on dual fuel reactivity controlled compression ignition (RCCI) in a light-duty engine operated with gasoline/diesel and methanol/diesel. *SAE Int. J. Engines* **2013**, *6*, 78–100.
13. Curran, S.J.; Cho, K.; Briggs, T.E.; Wagner, R.M. Drive cycle efficiency and emissions estimates for reactivity controlled compression ignition in a multi-cylinder light-duty diesel engine. In Proceedings of the Internal Combustion Engine Division Fall Technical Conference, Morgantown, WV, USA, 2–5 October 2011; Volume 44427.
14. Splitter, D.; Hanson, R.; Kokjohn, S.; Reitz, R.D. *Reactivity Controlled Compression Ignition (RCCI) Heavy-Duty Engine Operation at Mid-and High-Loads with Conventional and Alternative Fuels*; SAE Technical Paper No. 2011-01-0363; SAE International: Warrendale, PA, USA, 2011.

15. Curran, S.; Hanson, R.; Wagner, R. *Effect of E85 on RCCI Performance and Emissions on a Multi-Cylinder Light-Duty Diesel Engine*; SAE Technical Paper No. 2012-01-0376; SAE International: Warrendale, PA, USA, 2012.
16. Hanson, R.; Curran, S.; Wagner, R.; Reitz, R. Effects of biofuel blends on RCCI combustion in a light-duty, multi-cylinder diesel engine. *SAE Int. J. Engines* **2013**, *6*, 488–503.
17. Reitz, R.D. Directions in internal combustion engine research. *Combust. Flame* **2013**, *160*, 1–8.
18. Tripathi, G.; Dhar, A. Performance, emissions, and combustion characteristics of methane-diesel dual-fuel engines: A review. *Front. Therm. Eng.* **2022**, *2*, 870077.
19. Yoon, M.; Choi, M.; Kang, K.; Oh, C.; Park, Y.; Choi, G. Effects of n-Heptane/Methane Blended Fuel on Ignition Delay Time in Pre-Mixed Compressed Combustion. *Energies* **2022**, *15*, 4081.
20. Jia, Z. Dual-Fuel Combustion in a Heavy-Duty Engine. Ph.D. Thesis, Chalmers Tekniska Hogskola, Gothenburg, Sweden, 2018.
21. Doosje, E.; Willems, F.; Baert, R. *Experimental Demonstration of RCCI in Heavy-Duty Engines Using Diesel and Natural Gas*; SAE Technical Paper No. 2014-01-1318; SAE International: Warrendale, PA, USA, 2014.
22. Ryan, Walker, N.; Wissink, M.L.; DelVescovo, D.A.; Reitz, R.D. Natural gas for high load dual-fuel reactivity controlled compression ignition in heavy-duty engines. *J. Energy Resour. Technol.* **2015**, *137*, 042202.
23. Pedrozo, V.B.; Wang, X.; Guan, W.; Zhao, H. The effects of natural gas composition on conventional dual-fuel and reactivity-controlled compression ignition combustion in a heavy-duty diesel engine. *Int. J. Engine Res.* **2022**, *23*, 397–415.
24. Paykani, A.; Kakaee, A.H.; Rahnama, P.; Reitz, R.D. Effects of diesel injection strategy on natural gas/diesel reactivity controlled compression ignition combustion. *Energy* **2015**, *90*, 814–826.
25. Wu, Z.; Rutl, C.J.; Han, Z. Numerical evaluation of the effect of methane number on natural gas and diesel dual-fuel combustion. *Int. J. Engine Res.* **2019**, *20*, 405–423.
26. Nieman, D.E.; Dempsey, A.B.; Reitz, R.D. Heavy-duty RCCI operation using natural gas and diesel. *SAE Int. J. Engines* **2012**, *5*, 270–285.
27. Ansari, E.; Shahbakhti, M.; Naber, J. Optimization of performance and operational cost for a dual mode diesel-natural gas RCCI and diesel combustion engine. *Appl. Energy* **2018**, *231*, 549–561.
28. Ebrahimi, M.; Najafi, M.; Jazayeri, S.A. Artificial neural network to identify RCCI combustion mathematical model for a heavy-duty diesel engine fueled with natural gas and diesel oil. *J. Braz. Soc. Mech. Sci. Eng.* **2018**, *40*, 407.
29. Kakaee, A.H.; Nasiri-Toosi, A.; Partovi, B.; Paykani, A. Effects of piston bowl geometry on combustion and emissions characteristics of a natural gas/diesel RCCI engine. *Appl. Therm. Eng.* **2016**, *102*, 1462–1472.
30. Wang, B.; Li, T.; Ge, L.; Ogawa, H. Optimization of combustion chamber geometry for natural gas engines with diesel micro-pilot-induced ignition. *Energy Convers. Manag.* **2016**, *122*, 552–563. [CrossRef]
31. Liu, J.; Ma, B.; Zhao, H. Combustion parameters optimization of a diesel/natural gas dual fuel engine using genetic algorithm. *Fuel* **2020**, *260*, 116365.
32. Shirvani, S.; Shirvani, S.; Jazayeri, S.A.; Reitz, R. Optimization of the exergy efficiency, exergy destruction, and engine noise index in an engine with two direct injectors using NSGA-II and artificial neural network. *Int. J. Engine Res.* **2023**, *24*, 579–594.
33. Moradi, J.; Gharehghani, A.; Aghahasani, M. Application of machine learning to optimize the combustion characteristics of RCCI engine over wide load range. *Fuel* **2022**, *324*, 124494.
34. Richards, K.J.; Senecal, P.K.; Pomraning, E. *CONVERGE Manual 3.0*; CONVERGE: Manila, Philippines, 2020.
35. Han, Z.; Reitz, R.D. Turbulence modeling of internal combustion engines using RNG κ-ε models. *Combust. Sci. Technol.* **1995**, *106*, 267–295.
36. Wang, B.L.; Miles, P.C.; Reitz, R.D.; Han, Z.; Petersen, B. *Assessment of RNG Turbulence Modeling and the Development of a Generalized RNG Closure Model*; SAE Technical Paper No. 2011-01-0829; SAE International: Warrendale, PA, USA, 2011.
37. Issa, R.I. Solution of the implicitly discretised fluid flow equations by operator-splitting. *J. Comput. Phys.* **1986**, *62*, 40–65.
38. Beale, J.C.; Reitz, R.D. Modeling spray atomization with the Kelvin-Helmholtz/Rayleigh-Taylor hybrid model. *At. Sprays* **1999**, *9*, 623–650.
39. Reitz, R. Modeling atomization processes in high-pressure vaporizing sprays. *At. Spray Technol.* **1987**, *3*, 309–337.
40. Frassoldati, A.; D'Errico, G.; Lucchini, T.; Stagni, A.; Cuoci, A.; Faravelli, T.; Onorati, A.; Ranzi, E. Reduced kinetic mechanisms of diesel fuel surrogate for engine CFD simulations. *Combust. Flame* **2015**, *162*, 3991–4007.
41. Yousefi, A.; Guo, H.; Birouk, M. An experimental and numerical study on diesel injection split of a natural gas/diesel dual-fuel engine at a low engine load. *Fuel* **2018**, *212*, 332–346.
42. Senecal, P.K.; Pomraning, E.; Richards, K.J.; Briggs, T.E.; Choi, C.Y.; McDavid, R.M.; Patterson, M.A. Multi-dimensional modeling of direct-injection diesel spray liquid length and flame lift-off length using CFD and parallel detailed chemistry. *Sae Trans.* **2003**, *112*, 1331–1351.
43. Rahimi, A.; Fatehifar, E.; Saray, R.K. Development of an optimized chemical kinetic mechanism for homogeneous charge compression ignition combustion of a fuel blend of n-heptane and natural gas using a genetic algorithm. *Proc. Inst. Mech. Eng. Part D J. Automob. Eng.* **2010**, *224*, 1141–1159; Erratum in *Proc. Inst. Mech. Eng. Part D J. Automob. Eng.* **2011**, *225*, 1098.

44. Frössling, N. *Evaporation, Heat Transfer, and Velocity Distribution in Two-Dimensional and Rotationally Symmetrical Laminar Boundary-Layer Flow*; Fysiografiska Saellskapets Handlingar 51.NACA-TM-1432; NASA: Washington, DC, USA, 1958.
45. Post, S.L.; Abraham, J. Modeling the outcome of drop–drop collisions in Diesel sprays. *Int. J. Multiph. Flow* **2002**, *28*, 997–1019.
46. Schmidt, D.P.; Rutl, C.J. A new droplet collision algorithm. *J. Comput. Phys.* **2000**, *164*, 62–80.
47. Gonzalez, D.; Manuel, A.; Lian, Z.W.; Reitz, R.D. Modeling diesel engine spray vaporization and combustion. *SAE Trans.* **1992**, *101*, 1064–1076.
48. Heywood, J. *Internal Combustion Engine Fundamentals*; McGraw Hill: New York, NY, USA, 2018.
49. Hiroyasu, H.; Kadota, T. Models for combustion and formation of nitric oxide and soot in direct injection diesel engines. *SAE Trans.* **1976**, *85*, 513–526.
50. Yousefi, A.; Guo, H.; Birouk, M.; Liko, B. On greenhouse gas emissions and thermal efficiency of natural gas/diesel dual-fuel engine at low load conditions: Coupled effect of injector rail pressure and split injection. *Appl. Energy* **2019**, *242*, 216–231.
51. Sener, R.; Yangaz, M.U.; Gul, M.Z. Effects of injection strategy and combustion chamber modification on a single-cylinder diesel engine. *Fuel* **2020**, *266*, 117122.
52. Şener, R.; Gül, M.Z. Optimization of the combustion chamber geometry and injection parameters on a light-duty diesel engine for emission minimization using multi-objective genetic algorithm. *Fuel* **2021**, *304*, 121379.
53. Master Engineering Complexity and Speed Up Product Development. Available online: https://engineering.esteco.com/modefrontier/ (accessed on 1 March 2025).
54. Yang, X.S. *Nature-Inspired Optimization Algorithms*; Academic Press: Cambridge, MA, USA, 2020.
55. Srinivas, N.; Deb, K. Muiltiobjective optimization using nondominated sorting in genetic algorithms. *Evol. Comput.* **1994**, *2*, 221–248.
56. Halis, S. An experimental study of operating range, combustion and emission characteristics in an RCCI engine fueled with iso-propanol/n-heptane. *Sustainability* **2023**, *15*, 10897. [CrossRef]
57. Dempsey, A.B.; Reitz, R.D. Computational optimization of reactivity controlled compression ignition in a heavy-duty engine with ultra low compression ratio. *SAE Int. J. Engines* **2011**, *4*, 2222–2239.

Disclaimer/Publisher's Note: The statements, opinions and data contained in all publications are solely those of the individual author(s) and contributor(s) and not of MDPI and/or the editor(s). MDPI and/or the editor(s) disclaim responsibility for any injury to people or property resulting from any ideas, methods, instructions or products referred to in the content.